Pergamon

Int. J. Heat Mass Transfer. Vol. 39, No. 9, pp. 1883–1897, 1996

0017–9310/96 $15.00+0.00

0017–9310(95)00271–5

Analysis of transport phenomena governing interfacial bonding and void dynamics during thermoplastic tow-placement

R. PITCHUMANI
Department of Mechanical Engineering, University of Connecticut, Storrs, CT 06269-3139, U.S.A.

S. RANGANATHAN,† R. C. DON and J. W. GILLESPIE, JR
Center for Composite Materials, University of Delaware, Newark, DE 19716-3144, U.S.A.

and

M. A. LAMONTIA
Advanced Material Systems, E.I. du Pont de Nemours and Company, Newark, DE 19716-6108, U.S.A.

(*Received* 22 *February* 1995 *and in final form* 10 *July* 1995)

Abstract—The thermoplastic automated tow-placement process offers the potential for cost-effective fabrication of composite parts via consolidation *in situ*, thus avoiding the costly autoclave consolidation. The degree of interfacial bonding between tow layers and the void content in the composite laminate directly affect the mechanical properties and performance of the products. Theoretical models for the physical phenomena governing interfacial bonding and void dynamics (growth and consolidation) during the process are presented, which constitute the core of a numerical process simulator. Simulation-based parametric studies are reported for the case of an AS-4/PEEK composite to illustrate the effects of several process conditions and placement head configurations on the resulting degree of bonding and final void content. The analysis provides valuable insight towards optimal process and placement head design.

1. INTRODUCTION

The use of high-performance thermoplastic matrix composites will become widespread as costs are reduced through the development of 'affordable manufacturing' methods. Prepreg tape lay-up is an established process for thermoset matrix composites, requiring post-lay-up consolidation and cure in an autoclave. Thermoplastic matrix composites, on the other hand, may be fabricated using non-autoclave processing methods *in situ* such as filament winding and tow-placement. Thermoplastic processes potentially offer high throughput, thereby reducing manufacturing costs. Thermoplastic filament winding and automated tow placement are being considered for several applications including aircraft wing and fuselage skins, frames, stringers, wing boxes, underwater and armored vehicles, large tanks and industrial rollers [1,2].

In this paper, we consider the thermoplastic tow-placement process for fabricating continuous fiber-reinforced composites. The process is described in detail in the next section. The dominant mechanisms involved in the process are: (1) *heat transfer*, occurring throughout the process and defining the temperature field influencing the other phenomena, (2) *intimate contact*, the development of interfacial area contact between the tow and the substrate layer, as *inter*-laminar voids are removed, (3) *healing* (or *autohesion*), the interdiffusion of polymer molecules across the interface between tows, (4) *consolidation/squeeze flow*, a mechanism by which the *intra*-laminar void content within the tows are reduced by application of force under a compaction device, (5) *void growth*, resulting from the high temperatures in the tows during the process and (6) *polymer degradation*, a cumulative effect of exposure of the polymer matrix to high temperatures during the process. The temperature field in the tows directly influences processes (2)–(6) above, and hence the final product quality.

Thermoplastic tape laying (where the tapes are relatively wide compared to the tows used in tow-placement) has been studied by many investigators in recent years [3–7]. However, these investigations have focused mainly on the heat transfer involved in the process, and on the use of different heating sources. Mantell and Springer [7] additionally accounted for the phenomena of intimate contact and healing in their models. Theoretical and semi-empirical models

† Presently Guest Scientist at the National Institute for Standards and Technology, Gaithersburg, MD, U.S.A.

NOMENCLATURE

Bi	top surface Biot number, defined as $Bi = h_t \cdot H/k_z$
C	specific heat [J kg^{-1} K^{-1}]
D_b	degree of interfacial bonding
D_c	degree of compaction $=(h_i - h_f)/h_i$
D_h	degree of healing
D_{ic}	degree of intimate contact
F	consolidation force [N]
h	instantaneous tow thickness [m]; composite surface heat transfer coefficient [W m^{-2} K^{-1}]
h_f	final tow thickness after consolidation [m]
h_i	initial tow thickness prior to consolidation [m]
H	composite thickness [m]
k	thermal conductivity [W m^{-1} K^{-1}]
L_c	contact length between the tow and the roller [m]
N_{ply}	number of plies
p_{atm}	atmospheric pressure [N m^{-2}]
p_f	fluid pressure outside a void in the microscopic void dynamics model [N m^{-2}]
p_g	pressure inside a void, [N m^{-2}]
P	pressure under the consolidation roller [N m^{-2}]
R, R_o	instantaneous and initial void radii [m]
R_r	roller radius [m]
S, S_o	instantaneous and initial radii of the resin shell surrounding a void [m]
t	time [s]
t_r	reptation time in the healing model [s]
T	temperature [°C]
T_∞	ambient temperature [°C]
T_r	consolidation roller temperature [°C]
v	components of velocity in the consolidation model [m s^{-1}]
v_f	instantaneous void content in the composite [%]
v_{fin}, v_{in}	final and initial void content in the tows [%]
V	line speed [m s^{-1}]
w	tow width [m]
x, y, z	coordinate axes.

Greek symbols

ρ	density [kg m^{-3}]
μ	viscosity [N s m^{-2}]
σ	surface tension between air and the thermoplastic melt [N m^{-1}]
τ	Lagrangian time, defined as $\tau = y/V$ [s].

Subscripts and superscripts

*	dimensionless quantity (superscript)
b	bottom surface of the composite in contact with the mandrel
t	top surface of the composite
L, R	left and right sides of the composite ($y = 0$, L in Fig. 1b)
x, y, z	along the respective coordinate directions.

for polymer intimate contact and healing have also been developed by Agarwal [8], and Bastien and Gillespie [9], in the context of thermoplastic composite processing as well as thermoplastic welding. The kinetics of thermal degradation of polymer molecules exposed to high temperatures are generally described by an Arrhenius-type rate equation, and are reported in the literature [10–12]. Polymer degradation during the thermoplastic tow-placement process was investigated by the authors in a previous study [13].

The void content in the composite, and the amount of interfacial bonding between tows play an important role in determining the properties and performance of the products. It is evident from the foregoing discussion that the available process models account for only four of the six phenomena enumerated above namely, heat transfer, polymer degradation, healing, and intimate contact. The mechanisms of void reduction (consolidation) and growth have not been considered, and need to be included in the process simulations for an evaluation of the final void content. Furthermore, although healing and intimate contact have been modeled as independent mechanisms in the literature, estimation of the interfacial bond strength development during the process requires a coupled analysis of these two mechanisms, since the establishment of interfacial area contact is a prerequisite for initiation of healing.

The objectives of the paper are therefore: (1) to develop models describing void dynamics (growth and reduction) during the process, (2) to develop an integrated process simulator accounting for the interactions among the various mechanisms and (3) to illustrate the effects of several key process parameters on the product quality, primarily in regard to the void content and the degree of interfacial bonding. In the present study, void consolidation is modeled as a squeeze flow of a compressible fiber–resin–voids mixture under the compaction rollers [14], while void growth in the regions outside the consolidation zone is described as the expansion of the voids in a quiescent polymer melt at ambient pressure and at the temperature of the tow. In addition to the void consolidation and growth models, a transient heat trans-

fer model is also presented for the process, although the results are discussed pertaining only to the steady state operation of the process. The thermal and void dynamics models, along with the models for intimate contact, healing, and polymer degradation, form the integrated model base, which accounts for the interactions among the various mechanisms, and allows for a complete process simulation. Considering the case of an AS-4 graphite fiber reinforced poly-ether–ether–ketone (PEEK) matrix composite, process simulations were carried out for a wide range of operating conditions and for different placement head configurations. The results of the parametric studies are presented and discussed, which offer valuable information towards an optimum process and head design.

2. PROCESS DESCRIPTION

Figure 1(a) shows a schematic illustration of a tow-placement process, as considered in this study. In this process, a thermoplastic impregnated tow is passed under a lay-down roller [Roller 1 in Fig. 1(a)], onto a substrate formed of previously deposited and consolidated tows on a flat or a cylindrical mandrel, generically referred to as a mandrel throughout the paper. The substrate layer of tows is preheated by means of a preheat torch (Torch 1) prior to addition of the new tow, as shown in the figure. The tow-substrate assembly travels under a main torch (Torch 2), and subsequently under a compaction device, which in the present case is a roller (Roller 2), where the mechanisms of intimate contact, healing, and void removal by consolidation take place. The fully consolidated structure emerges from under Roller 2, ready to form the substrate for new tows added during the subsequent passes of the process. The rollers and torches, along with the supply spool, are mounted on a common frame, called the tow-placement head, and a translational line speed, V (assumed constant in this study), is maintained between the head and the tows throughout the process.

The schematic in Fig. 1(a) corresponds to the hardware configuration of the robotic fiber placement cell at the Center for Composite Materials, described in detail in ref. [15]. The regions of activity of the dominant physical mechanisms mentioned previously are as follows: (1) *heat transfer* takes place throughout the process; (2) *polymer degradation* occurs throughout the process, and is particularly of concern at the tow surface, which is exposed to the hot gas streams from the torches; (3) *intimate contact* is restricted to the regions under rollers with non-zero forces, i.e. Roller 2 in the case of single-roller consolidation, and Rollers 1 and 2 in the case of multi-roller con-

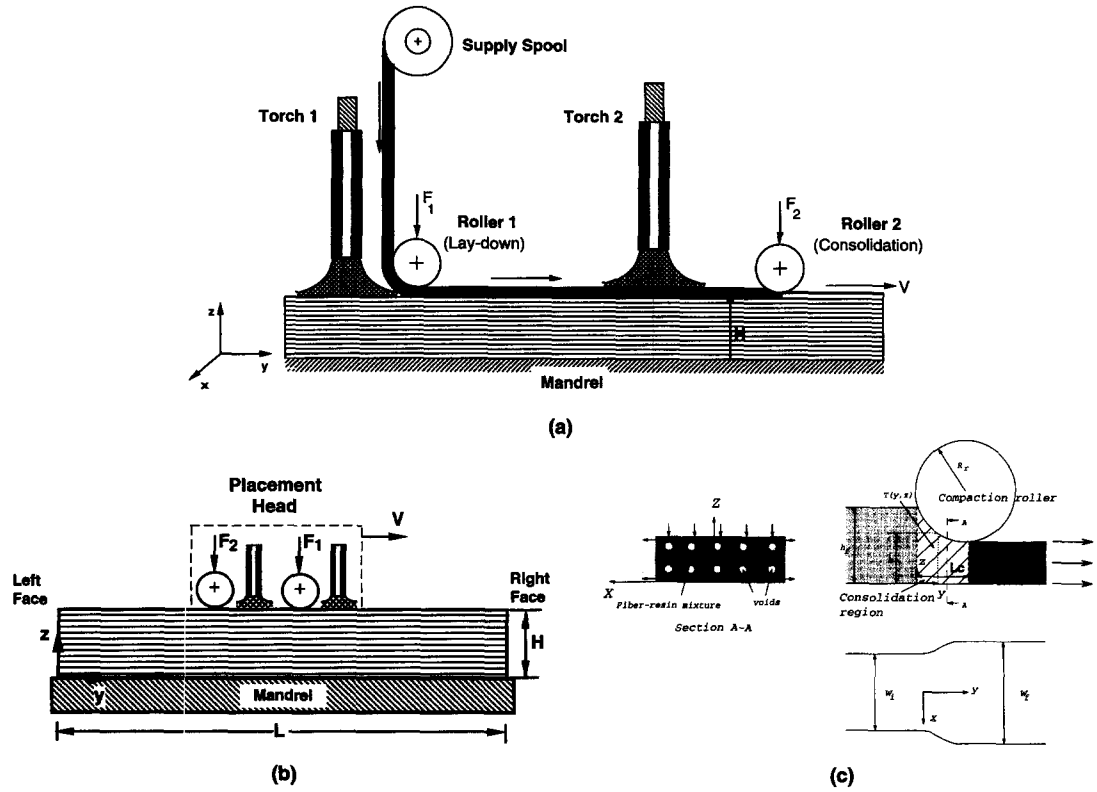

Fig. 1. (a) Schematic of the tow-placement process, (b) geometry of the problem domain used in the theoretical modeling and (c) enlarged view of the region under the compaction roller showing the consolidation process.

solidation; (4) *healing* takes place across areas in intimate contact that are above the critical temperature required for molecular interdiffusion (which for semi-crystalline materials is their melting point); however, unlike the mechanism of intimate contact, healing is independent of the applied force, and proceeds even beyond the roller exit; (5) *consolidation (squeeze flow)*, like intimate contact, occurs under the rollers with non-zero forces; and (6) *void growth* takes place in the regions prior to, and following the consolidation roller, as long as the tow temperature exceeds the glass transition temperature of the polymer.

Physical models for the mechanisms of heat transfer, and void consolidation and growth, as well as for the evolution of inter-laminar bond strength based on intimate contact and healing are described in the following sections. Polymer degradation is outside the focus of this paper, and is discussed elsewhere [13].

3. PROCESS MODELS

3.1. *Heat transfer*

The heat transfer model determines the transient temperature field within the tow layers, which is utilized in the analysis of the other mechanisms involved in the process. The thermal model consists of numerically solving the time-dependent energy equation in Cartesian coordinates, subject to the simplification that heat transfer due to the polymer crystallization process is negligibly small in comparison to the conduction heat transfer through the material. An exact analysis of the process requires consideration of three regions (the incoming prepreg tow, the substrate region prior to the lay-down roller and the laminate region following the lay-down roller) separately and ensuring temperature and heat flux continuities at the region boundaries.† In the interest of simplifying the geometry of the problem domain, it is assumed that the incoming tow is instantaneously laid down all along the substrate length, whereby the problem geometry is reduced to a single rectangular domain of length L, and thickness, H. In this simplification, the preheater torch heats the top surface of the incoming tow, as shown schematically in Fig. 1(b), instead of the top surface of the substrate, as in the actual process [Fig. 1(a)]. This assumption results in a lower estimate of the interface temperature under the lay-down roller (Roller 1), which in turns leads to a conservative evaluation of the bonding in those cases where Roller 1 is used for consolidation. As will be shown later in this article, this assumption is not severely restrictive since the preheater torch temperature has a relatively minor effect on the product quality in comparison to the main heater torch.

Using the above simplifications, the governing equation may be written as follows:

$$\frac{\partial}{\partial t}(\rho CT) = \frac{\partial}{\partial y}\left(k_y \frac{\partial T}{\partial y}\right) + \frac{\partial}{\partial z}\left(k_z \frac{\partial T}{\partial z}\right) \tag{1}$$

where T is the temperature in the composite, ρ, C, k are respectively the effective density, specific heat, and thermal conductivity of the tows, t is the time measured from the instant the placement head touches the lay-up, y is the distance along the lay-down direction, measured from the left face of the lay-up in Fig. 1(b) as the origin, z is the through-the-thickness coordinate, measured from the bottom surface of the laminate in contact with the mandrel as the origin.

Equation (1) is subject to an initial temperature field in the lay-up, given by: $T(y, z, 0) = T_o(y, z)$. The boundary conditions associated with equation (1) are generalized convective conditions on the top and bottom surfaces, and the sides of the tow assemblage, as given below.

$$-k_z \frac{\partial T}{\partial z}(z = 0) = h_b(T(z = 0) - T_{\infty b}(y,t))$$

$$-k_z \frac{\partial T}{\partial z}(z = H) = h_t(T(z = H) - T_{\infty t}(y,t)) \tag{2a}$$

$$-k_y \frac{\partial T}{\partial y}(y = 0) = h_L(T(y = 0) - T_{\infty L}(z,t))$$

$$-k_y \frac{\partial T}{\partial y}(y = L) = h_R(T(y = L) - T_{\infty R}(z,t)) \tag{2b}$$

where h is the convective heat transfer coefficient and T_∞ is the ambient temperature. The subscripts b, t, L and R refer to the bottom and top surfaces, and the left and right faces of the lay-up [$y = 0$, and L in Fig. 1(b)], respectively. The symbol H in equation (2a) is the composite thickness [Fig. 1(b)]. The ambient temperatures on the top surface, $T_{\infty t}$, used in the present study were those measured experimentally during typical processing runs on a small-scale robotic tow-placement facility at the Center for Composite Materials [13]. Furthermore, in the calculations presented in this paper, the convective heat transfer coefficient on the bottom surface, h_b, is set to be ∞, to simulate a perfect contact with the mandrel (i.e. $T(y, z = 0, t) = T_{\infty b}$).

The top surface heat transfer coefficient, h_t, is a function of the axial location, y. Since the rollers are in contact with the tow surface under the action of an external force, perfect contact ($h_t = \infty$) is assumed between the roller and the top surface of the tow. The heat transfer under the torches is that of forced convection due to the impingement of hot gases onto the moving tow, while the heat transfer in the regions between the torches and the rollers, and outside the placement head region is due to free convection. In the present analysis, the heat transfer coefficients were estimated from experimental measurements of the

† Such a model is presently being developed and will be reported in a forthcoming publication.

tow-surface and ambient temperatures during the process. A look-up table of heat transfer coefficients was then created for use in the theoretical studies. Since the thicknesses of the laminates considered in this study are small in comparison to the lay-up length, heat loss from the left and right faces of the lay-up is expected to be generally negligible. Accordingly, the heat transfer coefficients on the left and right faces of the laminate (h_L and h_R) were set to zero in the computations.

The thermal model yields the transient temperature field as a function of the spatial location within the composite. However, since the focus of this article is on the steady-state operation of the process, the steady-state temperature profile in the composite is of relevance in the analysis of the other mechanisms involved in the process. Accordingly, the remainder of the process submodels presented in this section are restricted to a steady-state formulation.

3.2. *Void consolidation*

In the case of thermoset matrix composites, owing to their relatively low viscosity prior to cure initiation, consolidation can be modeled as flow of resin through a porous network of fibers, which is described well by Darcy's law. Thermoplastics, however, exhibit a high viscosity as a result of which the fibers move along with the resin, rather than relative to the resin. Therefore, the process may be best described as a squeeze flow as opposed to a Darcian flow. The fiber–resin–voids mixture is modeled as an equivalent homogeneous fluid with the rheological properties of the continuum dependent on the temperature, the fiber volume fraction and the void content.

The dominant consolidation-related void dynamics mechanisms modeled in this study are those of void migration along with the resin and void compression due to the effects of cooling, and compaction under the applied pressure. The diffusion of gases across the void–tow melt interface is assumed to be negligible in the present analysis. The effect of void migration is accounted for in a *macroscopic* flow model, while the void compression effects are considered in a *microscopic* void dynamics model. These two models are coupled and necessitate a simultaneous solution for the void fraction in the composite.

3.2.1. *Macroscopic void transport model.* Figure 1(c) shows an enlarged view of the consolidation region under a compaction roller. In the consolidation step, a tow of a given height, h_i, and width, w_i, enters the region under the roller with a specified line speed, V. The tow undergoes void compression due to the applied consolidation force, and its height reduces to h_f while its width increases to w_f. Since the tow dimension in the y-direction is much larger than the x- and z-dimensions, flow in the y-direction may be neglected. Further, owing to the high viscosity of the matrix resin, the inertial effects may be neglected and the consolidation process may be treated as a creeping flow problem.

The fluid motion under the compaction roller is governed by the continuity and momentum equations in Cartesian coordinates. In actual tows, since the thickness (typically 0.006 in) is much smaller than the width (typically 0.25 in), the dominant velocity gradient terms in the momentum equations are the shear strain rate through the gap, $\partial v/\partial z$, and its derivative with respect to the thickness direction, z. The continuity equation and the simplified momentum equations for the squeeze flow may then be written in a *Lagrangian* form as,

$$\frac{\partial \rho}{\partial \tau} + \frac{\partial}{\partial x}(\rho v_x) + \rho \frac{\partial v_z}{\partial z} = 0 \tag{3}$$

$$\frac{\partial P}{\partial x} = \frac{\partial}{\partial z}\left(\mu \frac{\partial v_x}{\partial z}\right) \quad \text{and} \quad \frac{\partial P}{\partial z} = 0. \tag{4}$$

In the above equations, v denotes the flow velocity, and its subscripts refer to the direction of the velocity. The symbol τ is the Lagrangian time which is related to the line speed, V, and the location under the roller (measured from the entrance to the roller region), y, as $\tau = y/V$. The continuity equation, equation (3), assumes that the density is a function of x and τ only, and the momentum equations, equation (4), suggest that the pressure is also a function of x and τ only. The viscosity, μ, of the fluid is evaluated using an Arrhenius-type correlation of the form [7],

$$\mu = A \cdot \exp\left(\frac{B}{T}\right) \tag{5}$$

where A and B are empirically determined constants. For the AS-4/PEEK system, $A = 132.95\ \text{N s m}^{-2}$ and $B = 2969$ K [7]. Note that the viscosity relationship holds only for temperatures exceeding the glass transition point, T_g. Below this limit, the matrix material remains a solid and the void dynamics mechanisms are arrested.

Integrating the continuity equation, equation (3), across the instantaneous thickness of the tow, i.e. from 0 to h, and substituting for $v_z(z = 0) = 0$ and $v_z(z = h) = \mathrm{d}h/\mathrm{d}\tau$, the rate of compaction of the tows, one obtains:

$$h\frac{\partial \rho}{\partial \tau} + \frac{\partial}{\partial x}\left(\rho \int_0^h v_x \, \mathrm{d}z\right) + \rho \frac{\mathrm{d}h}{\mathrm{d}\tau} = 0 \tag{6}$$

where Leibnitz rule [16] has been used to re-express the integral of the x-derivative term in the continuity equation.

The momentum equation in the x-direction may be integrated twice across the thickness of the tow, to obtain an expression for the velocity component, v_x. Substituting the resulting expression for v_x into equation (6), we obtain the following general form of the *macroscopic* governing equation for determining the pressure distribution under the roller,

$$h\frac{\partial\rho^*}{\partial\tau}+\rho^*\frac{dh}{d\tau}+\frac{\partial}{\partial x}\left(\rho^*\int_0^h\left[v_x(0)+\frac{dP}{dx}\int_0^z\frac{\xi}{\mu}d\xi+C_1(x)\int_0^z\frac{1}{\mu}d\xi\right]dz\right)=0 \quad (7)$$

where ξ is a dummy variable of integration, $C_1(x)$ is a constant of integration from the velocity profile, and ρ^* is the density of the fiber–resin–voids mixture scaled with respect to the density of the mixture in the absence of voids.

Since equation (7) involves the second derivative of pressure with respect to x, two pressure boundary conditions are required to solve the equation. Assuming the tow to be unconstrained along its sides, the appropriate pressure conditions are simply $P(x=\pm w/2)=p_{atm}$, the atmospheric pressure. The terms within square brackets in equation (7) denote the expression for $v_x(z)$. The unknowns $v_x(0)$ and $C_1(x)$ in the expression are determined using the velocity boundary conditions at $z=0$ (tow-substrate interface) and $z=h$ (tow-roller contact). The boundary conditions may be written in a generalized form as: $(\partial v_x/\partial z)_{z=0}=K_b/\mu\cdot v_x(0)$ and $(\partial v_x/\partial z)_{z=h}=K_t/\mu\cdot v_x(h)$, where K_b/μ and K_t/μ are parameters that determine the type of velocity boundary condition at the two–substrate and tow–roller interface, respectively. A value of K_b/μ or $K_t/\mu=\infty$ implies a no-slip condition, i.e. $v_x(z=0)=0$, whereas a value of 0 corresponds to a perfect slip condition. In the present case, a no-slip condition exists at the tow–substrate interface, i.e. $K_b/\mu=\infty$, while a condition of partial slip tending towards complete slip exists at the tow–roller interface, i.e. $K_t/\mu\approx 0$.

Equation (7) and the pressure and velocity conditions constitute the *macroscopic* model. The solution of the *macroscopic* model equations for the pressure profile requires the expressions for the closing speed between the compacting surfaces, $dh/d\tau$, and the time derivative of the dimensionless density, $\partial\rho^*/\partial\tau$. The closing speed is determined from geometric considerations, while the dimensionless density is obtained from a *microscopic* model which accounts for the void dynamics during the consolidation process.

From geometric considerations, the instantaneous tow thickness, h, is related to the under-roller distance, y, as: $h=R_r+h_f-[R_r^2-(L_c-y)^2]^{1/2}$, where R_r is the consolidation roller radius and L_c is the contact length under the roller in Fig. 1(c), given by $L_c^2=R_r^2-(R_r-h_i+h_f)^2$. All the other terms are as defined previously. Differentiating the expression for h with respect to τ, and setting $dy/d\tau=V$, the following expression emerges for the closing speed.

$$\frac{dh}{d\tau}=-V\frac{[R_r^2-(R_r-h+h_f)^2]^{1/2}}{(R_r-h+h_f)}. \quad (8)$$

The width change corresponding to a thickness compaction can be determined from mass conservation.

3.2.2. *Microscopic void consolidation model.* A typical void at any location may be approximated by a sphere of radius R, surrounded by a concentric spherical resin shell of outer radius S. The ratio of R and S is determined by the void fraction at the location under consideration. Void growth or collapse is governed by a balance between the pressure inside and outside the void, and the surface tension (σ) and the resin viscosity (μ) [17],

$$4\mu\left(\frac{R^{*3}}{S^{*3}}-1\right)\frac{dR^*}{dt}+(p_g-p_f)R^*-2\sigma/R_o=0 \quad (9)$$

where the bubble and outer shell radii are scaled with respect to the initial radius of the void, R_o, which is determined based on the void fraction in the tow at the entrance to the consolidation roller. In the above equation, the gas pressure inside the void is denoted as p_g, and the fluid pressure surrounding the void is labeled p_f.

Under assumption of an incompressible resin, conservation of resin mass in the outer shell yields the relationship: $S^{*3}-R^{*3}=S_o^{*3}-1$, where S_o^* is the dimensionless initial radius of the outer resin shell, scaled with respect to R_o. Also, from ideal gas law, we have: $p_{go}/T_o=p_gR^{*3}/T$, where p_g and p_{go} are the instantaneous and initial pressures inside the voids, respectively. Using these relationships, equation (9) may now be rewritten as follows, which is the *microscopic* void dynamics equation.

$$4\left(\frac{R^{*3}}{S_o^{*3}+R^{*3}-1}-1\right)\frac{dR^*}{d\tau}+\left(\frac{p_{go}}{R^{*3}}\frac{T}{T_o}-p_f\right)\frac{R^*}{\mu}-\frac{2\sigma}{\mu R_o}=0. \quad (10)$$

Further, it can be shown that the rate of change of ρ^* with respect to time can be expressed in terms of the rate of change of the non-dimensional radius of void as [14],

$$\frac{\partial\rho^*}{\partial\tau}=\frac{-3R^{*2}(S_o^{*3}-1)}{(S_o^{*3}-1+R^{*3})^2}\frac{dR^*}{dt}. \quad (11)$$

For a set of given initial conditions on the void radii, density, pressure and temperature, the rate of change of the non-dimensional density with respect to time may be obtained using equations (10) and (11). This expression may be used in equation (7) to compute the pressure distribution in the consolidation region. Equation (10) can then be used to compute the change in radius of the voids, and update the void radius at various locations in the domain. Similarly, equation (11) may be integrated numerically to obtain the local densities in the tow as a function of x and τ.

3.3. *Void growth*

In the regions outside the consolidation rollers, the tow matrix melt is exposed to the ambient atmospheric pressure (i.e. $p_f=p_{atm}$). The reduced fluid pressure outside the voids, combined with the high void pres-

sures (resulting from the high temperatures under the torches) causes the voids to grow in size. Furthermore, since the tow surfaces are unconstrained and the matrix melt is assumed incompressible, the increase in the void size leads to an increase in the tow dimensions. The goal of the void growth analysis is therefore that of determining the void fraction and tow thickness as a function of the axial location along the process [y-direction in Fig. 1(a)].

Since the fluid pressure is known (ambient), the *macroscopic* model equations need not be solved in the void growth analysis. The change in the void dimensions is given by the *microscopic* model [equation (10)], with p_f replaced by p_{atm}, and the corresponding density change is obtained from equation (11). The instantaneous void fraction for the concentric void–resin shell model is then given by

$$v = \frac{R^{*3}}{S_o^{*3} + R^{*3} - 1}. \tag{12}$$

Since the tow is bonded to the substrate along its width, the tow volume change due to void growth translates to a tow thickness increase governed by: $h \cdot (1 - v) = \text{constant}$.

3.4. *Interfacial bonding*

Interfacial bonding and the development of bond strength during the process are attributed to the mechanisms of intimate contact and healing at the tow–substrate interface. Theoretical models for the two mechanisms are briefly reviewed below, followed by a discussion on the coupling of the two mechanisms towards evaluation of the bond strength in the composite.

3.4.1. *Intimate contact.* The mechanism of intimate contact is dependent upon the relative surface roughness (asperities), the temperature profile, and the pressure field at the interface between the freshly deposited tow and the top surface of the substrate. The intimate contact model employed in the study follows that presented by Mantell and Springer [7], with the important distinction that the actual pressure and temperature profiles under the roller, obtained from the consolidation and thermal models, respectively, are used in place of an average roller pressure and an isothermal field as proposed in the original development. (By way of comparison, the degree of intimate contact evaluated based on the average pressure and an isothermal temperature field could be different by as much as 26% for nominal process settings.) The model idealizes the surface asperities of the tow as a periodic wave of rectangular elements that flatten out under the applied pressure. This results in a decrease in the element height and a simultaneous increase in its width (interfacial contact area). A degree of intimate contact, D_{ic}, is defined as the ratio of the instantaneous width of the rectangular asperity to the wavelength of the periodic arrangement. Physically, the term D_{ic} represents the fraction of interfacial area in intimate contact at any Lagrangian instant τ during the process. Thus, a value of $D_{ic} = 1$ denotes complete intimate contact. Based on experimental measurements of the smooth and rough regions of tow surfaces, a semi-empirical model may be fit as follows

$$D_{ic}(\tau_{ic}) = 0.29\left[\int_0^{\tau_{ic}} \frac{P}{\mu} d\tau\right]^{1/5}. \tag{13}$$

Equation (13) assumes that the fiber–matrix material behaves as a Newtonian fluid in laminar flow under an applied pressure, P. The other terms appearing in the above equation are as follows: μ is the temperature-dependent fiber–matrix viscosity given by equation (5) and τ_{ic} is the time available for intimate contact under the rollers.

3.4.2. *Polymer healing.* Healing is a temperature-dependent phenomenon that is governed by the migration of polymer chains *across the interfacial areas in intimate contact.* Full healing across the interface between the deposited tow and substrate is essential to obtain a bond with maximum performance. The healing model employed in this study is that of Bastien and Gillespie [9], as applied by Agarwal [8] for PEEK-based thermoplastic composites. By applying a shift factor, a_T, to the reptation time, t_r^*, at a reference temperature, T_{ref}, the non-isothermal healing model based on strength considerations is as follows:

$$D_h(\tau_h) = \left(\frac{1}{t_r^*}\right)^{1/4} \sum_{j=1}^{\tau_h/\Delta\tau} \left[\frac{(\tau_j)^{1/4} - (\tau_{j-1})^{1/4}}{a_T(T_j)^{1/4}}\right]$$

$$a_T(T) = \exp\left[\frac{E_a}{R}\left(\frac{1}{T} - \frac{1}{T_{ref}}\right)\right]. \tag{14}$$

In the above equation, D_h is the degree of healing of the polymer at a time instant τ, E_a is the activation energy of diffusion of the polymer, R is the universal gas constant and τ_h is the time for the healing process, which is discretized into intervals of duration, $\Delta\tau$. Complete healing in terms of strength is defined as the point when the degree of healing attains a value of unity. For PEEK, the following values of the constants apply [8]: $E_a = 57.3$ kJ mol^{-1}, $t_r^* = 0.11$ s at $T_{ref} = 400$°C. Furthermore, it is assumed that healing occurs above the melt temperature where the polymer chains are free to migrate and diffuse across the interface, but ceases completely upon cooling below a temperature of 280°C, the point at which PEEK crystallizes and the chains become rigidly fixed.

Note that due to its dependence on the pressure field, intimate contact develops only in the regions under the rollers with non-zero consolidation forces. Polymer healing, on the other hand, is a temperature-controlled phenomenon and continues to take place even after the externally applied force is removed. As a result, healing continues to progress even beyond the roller exit, as long as the low temperature exceeds the material melting point.

As explained previously, in general, the processes

of intimate contact and healing are coupled, in that intimate contact is a prerequisite for the initiation of healing. Considering a time interval between τ and $\tau+\Delta\tau$ during the process, the incremental dimensionless area that comes into intimate contact in this period is given by $(\mathrm{d}D_{ic}/\mathrm{d}\tau)\cdot\mathrm{d}\tau$. The extent of healing for this incremental area, observed at a final time τ_h, may be denoted as $D_h(\tau_h-\tau)$, where $\tau_h-\tau$ is the time duration available for the incremental area to heal. The net bond strength developed at the interface after a time τ_h is an area average of the bond strengths of each of the incremental areas, and may be expressed in a dimensionless form as follows:

$$D_b(\tau_h)=\int_0^{\tau_{ic}} D_h(\tau_h-\tau)\cdot\frac{\mathrm{d}D_{ic}}{\mathrm{d}\tau}(\tau)\,\mathrm{d}\tau. \qquad (15)$$

In the above equation, D_b is the interfacial bond strength scaled with respect to the maximum realizable bond strength in the composite. The degree of healing function, D_h, is evaluated using equation (14) with τ replaced by $\tau_h-\tau$ on the right-hand side of the equation, and $\mathrm{d}D_{ic}/\mathrm{d}\tau$ is obtained by replacing τ_{ic} with τ in equation (13), and differentiating the resulting expression with respect to τ. Further discussion on the bonding model and its characteristics may be found in ref. [18].

In the tow-placement process, the residence time of the tows under the consolidation roller, τ_{ic}, which is also the time that is available for intimate contact to develop, is small in comparison to the time available for healing to occur, τ_h. For example, at nominal operating conditions, the time under the rollers is typically on the order of 0.05 s, while the time available for healing is on the order of 1 s. Therefore, $D_h(\tau_h-\tau)$ with $0\leqslant\tau\leqslant\tau_{ic}$ may be approximated as $D_h(\tau_h)$. By virtue of this simplification, the degree of bonding (equation (15)) may be expressed, approximately, as follows:

$$D_b(\tau_h)\approx D_h(\tau_h)\cdot D_{ic}(\tau_{ic}). \qquad (16)$$

The above equation allows for a simplified, yet reasonably accurate evaluation of the degree of interfacial bonding without resorting to a rigorous numerical computation. This is especially advantageous in the use of the process simulator for purposes of model-based control, which demands quick response times from the models. The accuracy of the simplified evaluation was examined in a separate study [19] where the bond strengths predicted by equation (16) were shown to be in good agreement (to within about 10%) with the interlaminar shear strengths measured experimentally using short-beam shear tests. Since the focus of the present article is on the presentation of physical process models, the validation results are not repeated here. However, the reader is referred to ref. [19] for a discussion on the experimental studies. The results presented here are based on the simplified expression given in equation (16), which adequately serves to illustrate the physical trends in the strength values.

4. NUMERICAL SOLUTION PROCEDURE

Equation (1) and the associated initial and boundary conditions were solved for the temperature field using an Alternating Direction Implicit (ADI) scheme based on a control volume formulation, given in ref. [20]. The numerical scheme is second-order and first-order accurate, respectively, in the spatial and temporal discretizations. The time step was chosen such that the mesh Courant number $(V\cdot\Delta t/\Delta x)$ and the mesh Fourier numbers $(\alpha_y\Delta t/\Delta y^2,\ \alpha_z\Delta t/\Delta z^2)$ were all less than unity, which ensured that the time steps were small enough to resolve the characteristic time scales for thermal diffusion and advection. The solution of the governing equations and the associated boundary conditions yielded the transient temperature history in the composite. The steady-state portion of the temperature profile in the tows directly under the placement head was used in the analysis of the other dominant mechanisms.

The *macroscopic* and *microscopic* void consolidation model equations [equations (7) and (10)] were solved iteratively using a numerical procedure. An explicit finite difference scheme, with the spatial derivatives approximated by central differences, was utilized for solving the *macroscopic* pressure equation. A domain-adaptive discretization was employed which ensured conformity to the dimensional changes of the tow during the consolidation process. The integrals in the integro-differential pressure equation were evaluated using the Simpson's rule [16]. The *microscopic* void dynamics equation [equation (10)] used in both the void consolidation and the void growth models was solved using a fourth-order explicit Runge–Kutta method [16]. Furthermore, the void fractions reported in this paper are the width-averaged values, also obtained using Simpson's rule. Additional details of the solution method may be found in ref. [14].

For a specified degree of compaction, $D_c=(h_i-h_f)/h_i$, and incoming void fraction, v_{in}, the void consolidation model yields the pressure field under the roller, and the void content at the roller exit, evaluated using the information on the void radii [equation (12)]. The consolidation force, F, that needs to be applied on the roller to achieve the desired degree of compaction may then be calculated by integrating the under-roller pressure profile. For a practical implementation, however, the model needs to be inverted, where the consolidation force is specified and the corresponding degree of compaction and void fractions are calculated. The inversion was achieved in this study by means of an iterative procedure wherein the consolidation and void growth models were invoked along with the heat transfer model, for several systematic trial values of the degree of compaction (determined using a binary search algorithm in the range $0\leqslant D_c\leqslant 1$) until the consolidation force required matches the specified value. In all the computations, the temperature-dependent density and viscosity of the fluid were evaluated using the steady-

state temperature field in the consolidation region, obtained from the heat transfer model.

For a given set of process parameters, the simulation procedure consists of iteratively invoking the thermal and the void dynamics models, and obtaining the converged steady state thermal and pressure fields in the tows. The pressure and steady-state temperature values are then used in the intimate contact and healing submodels to determine the degrees of intimate contact (D_{ic}) and healing (D_h) at the tow–substrate interface. The degree of bonding is then estimated as the product of D_{ic} and D_h. The process simulator further yields a degree of polymer thermal degradation, based on the temperature history that tows are subjected to during the process and using the model presented in ref. [13]. The numerical process simulator is implemented on a Silicon Graphics workstation with a RISC 4000 CPU architecture. Process simulations were carried out for a wide range of processing conditions, in order to study the effects of the process variables on two of the product parameters of interest namely, the void content and the interfacial bond strength. A typical simulation nominally required on the order of a few minutes of CPU time for execution and the results of the simulations are discussed in the following section.

5. RESULTS AND DISCUSSION

The input parameters used in the simulations, and the simulation outputs are summarized in Table 1, where the hardware parameters correspond to those of the robotic tow-placement facility at the University of Delaware's Center for Composite Materials. Note that for most of the results examined in this section, the output values of interest are the final quantities at the exit of the placement head region (of axial length ≈ 0.12 m, i.e. at $\tau = 0.12/V$). The parametric studies are presented in terms of the degree of bonding, D_b, and the void fraction, v_f, in the composite product.

Since the temperature field directly influences bonding and void consolidation/growth phenomena, the typical variation of the steady state temperature at the tow–substrate interface is shown in Fig. 2(a) for three different line speeds. The profiles correspond to the region of the tows directly underneath the placement head (axial length ≈ 120 mm). The temperature profile exhibits two peaks corresponding to the two torches, and rapid cooling in the free convection zones as well as under the rollers. At lower speeds, the longer residence time in each zone results in higher peak temperatures, but also considerable heat loss in the free convection zones and under the rollers. At higher

Table 1. Process simulator inputs and outputs

Hardware configuration	
Roller 1 radius, R_{r1}	= 25.4 mm
Roller 2 radius, R_{r2}	= 25.4 mm
Roller 1 temperature, T_{r1}	= Isothermal @ tow temperature (single-roller consolidation) = 200°C (multi-roller consolidation)
Roller 2 temperature, T_{r2}	= 100°C
Prepreg tow parameters	
Material	AS4/PEEK
Initial void content, v_{in}	= 5%
Initial tow width, W	= 6.35 mm
Initial tow thickness, h_i	= 0.1778 mm
Material properties	
Viscosity, $\mu(T)$	(equation 5, ref. [7])
Surface tension, $\sigma(T)$	(ref. [21])
Density, ρ, specific heat, C_p, thermal conductivity, k (ref. [21])	
Glass transition temperature, T_g, melting point, T_{mp} (ref. [21])	
Process variables	
Number of plies, N_{ply}	= 10 (except Fig. 4a)
Line speed, V	
Consolidation forces: F_1, F_2	
Torch temperatures: T_1, T_2	
Mandrel temperature, $T_{\infty b}$	= 100°C
Simulator outputs	
Degree of bonding	$D_b(\tau)$
Void fraction	$v_f(\tau)$
Degree of degradation	$\alpha(\tau)$
Degree of compaction	$D_c(\tau)$
Temperature	$T(z, \tau)$

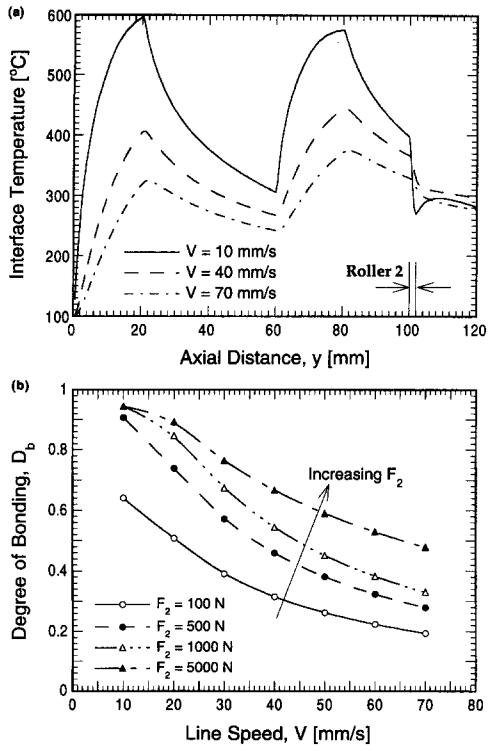

Fig. 2. (a) Variation of the steady state tow–substrate interface temperatures in the region directly underneath the placement head for three different processing speeds and (b) effect of compaction force on the degree of bonding as a function of the processing speed, for nominal heat inputs.

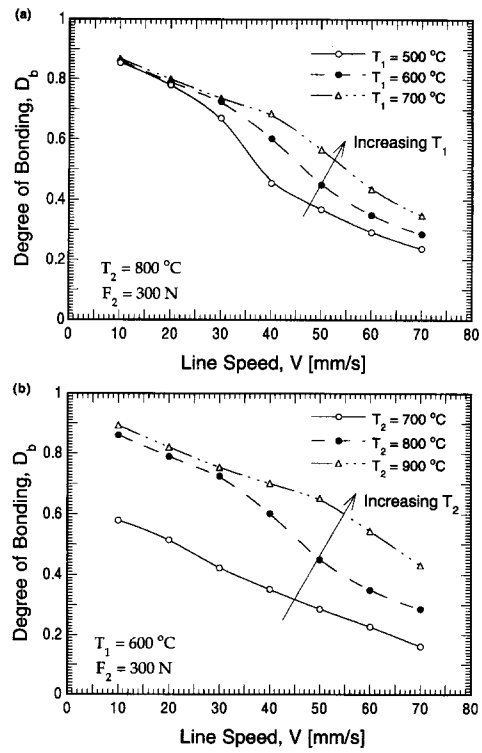

Fig. 3. Effect of (a) preheater and (b) main heater torch temperatures on the degree of bonding as a function of the processing speed.

speeds, the decrease in the residence time under the torches leads to reduced interface temperatures under the rollers.

5.1. *Interfacial bonding*

Figure 2(b) shows the effect of the compaction force, F_2, and the line speed, V, on the degree of bonding in the composite. It is seen that for a given consolidation force, the bond strength decreases with increasing line speed, which may be attributed to two factors: first, with increasing speed, as seen in Fig. 2(a), the temperatures in the tow are lower and consequently, the fluid viscosity is higher, leading to less consolidation and intimate contact. Moreover, at lower temperatures, the extent of healing is small which also contributes to the decrease in the bond strength. Secondly, higher speeds are characterized by smaller times available under the roller (equivalently, a smaller contact patch length) for intimate contact (and bonding) to develop. With increasing consolidation force for a given line speed, the resulting pressures under the roller are higher and therefore, better intimate contact is achieved leading to good bonding. Furthermore, with increasing force, more time is available for intimate contact (and bonding) to take place owing to the increased contact length under the roller.

Figure 3 examines the influence of the torch temperatures on the degree of bonding in the composite. In general, as the heat input is increased, the temperatures in the tows are higher which in turn leads to an increased degree of intimate contact as well as an enhanced degree of healing. As a result, the degree of bonding is expected to increase with increasing heat input from the torches. Figure 3(a) illustrates this point clearly for a 10-ply thick composite, where D_b is seen to increase with increasing preheater torch temperature, T_1. A similar trend is also observed with regard to the main heater torch temperature, T_2, in Fig. 3(b). However, a comparison between Figs. 3(a) and (b) reveal that the main heater torch temperature has a more pronounced effect on the degree of bonding than the preheater torch temperature, for the particular placement head configuration employing a single roller (Roller 2) consolidation used in these figures. This suggests that from a process control viewpoint, the main heater torch temperature is a very sensitive control variable.

Simulations were also carried out to investigate the consolidation process as tows are incrementally stacked to build up the composite thickness. The results of these simulations on the degree of bonding are shown in Fig. 4(a) as a function of line speed and as the number of plies, N_{ply}, is increased from 1 to 10. The mandrel temperature in all these simulations was held at 100°C, whereby the mandrel acted as a heat sink in the laying up of the first few plies. It was found

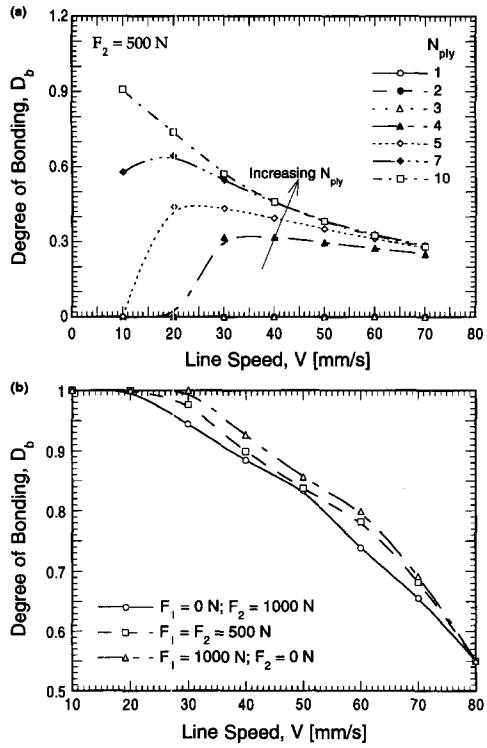

Fig. 4. (a) Variation of the degree of bonding profiles with increasing composite thickness, showing the existence of optimal processing speeds for maximized bonding; (b) effect of multi-roller compaction on the degree of bonding as a function of the processing speed, for nominal heat inputs.

from the simulations that for number of layers greater than 10 (and $V \geqslant 10$ mm s^{-1}), the mandrel temperature does not have any significant impact on the consolidation process. The results for $N_{ply} \geqslant 11$ are not shown in the plot for enhanced clarity, since they are almost coincident with the results for $N_{ply} = 10$.

Figure 4(a) shows that the degree of bonding generally increases from a value of 0 at low speeds, reaches a maximum and decreases with further increase in the line speed. This trend is especially pronounced for the first few layers, where there is a significant influence of the mandrel. For $N_{ply} \leqslant 3$, bonding remains uninitiated throughout the process, over the range of line speeds shown, since the interface temperature is less than the melting point of PEEK (280°C), which needs to be exceeded for polymer healing to occur. For the fourth layer ($N_{ply} = 4$), the interface temperature exceeds the melting point at speeds greater than about 20 mm s^{-1} due to the insufficient time available for the interface to be cooled by the mandrel. As a result, a finite bonding is achieved for $V > 20$ mm s^{-1}. However, at higher speeds, reduced temperatures in the composite [see Fig. 2(a)], coupled with the decrease in the contact time under the roller, causes the degree of bonding to eventually decrease at speeds greater than about 40 mm s^{-1}.

Thus, for a given number of plies, there exists an optimum range of V over which the degree of bonding is maximized. With increasing number of tow layers, the mandrel has a decreasing influence on the cooling of the tow-substrate interface, and both the critical speed for initiation of bonding as well as the optimum speed for maximized bonding shift toward lower values. Furthermore, with the increase in N_{ply}, the temperature in the composite increases and a higher degree of bonding is achieved. This is also evident in the experimental parts fabricated by this process, where the bottom few plies can be peeled off with just the nominal effort [19]. Process modifications using a heated or insulated mandrel may overcome this problem. However, the feasibility of these remedies for practical implementation needs to be explored before a recommendation can be made.

The discussion so far pertained to the case of consolidation under a single roller (Roller 2). However, as seen in the figures presented so far, the amount of bonding remains less than the maximum realizable in most of the cases, i.e. $D_b < 1$. In an attempt to improve the extent of bonding, one possible modification to the placement head configuration was explored, which is to use the lay-down roller [Roller 1 in Fig. 1(a)] also for consolidation, in conjunction with Roller 2. The results for this head configuration are presented in Fig. 4(b), where three different distributions of a net consolidation force of 1000 N are considered between the two rollers: (1) where the force is applied on Roller 2 only, (2) where the total force is distributed equally between the two rollers and (3) where the force is applied entirely on the first roller. In Case 2, which involves consolidation under two rollers, the degree of bonding was evaluated by accounting for the different healing histories that the incremental contact areas under the two rollers are subjected to during the process.

The results in Fig. 4(b) demonstrate that the degree of bonding can be increased by using the first roller for compaction, either individually or in conjunction with Roller 2, whereby intimate contact is initiated earlier on in the process, and longer time is provided for healing to take place. Moreover, the process of healing (and bond strength development) is accelerated as the tow passes under the main heater torch prior to reaching Roller 2. It is further seen that of the two cases that use Roller 1 for consolidation (Cases 2 and 3 above), consolidation entirely under Roller 1 (Case 3) results in a higher degree of bonding in comparison to the case of consolidation under both rollers (Case 2). This is due to the proximity of the first roller to the preheater torch region which leads to higher tow temperatures under the first roller. However, as will be seen later in this section, use of Roller 1 alone for compaction also leads to increased void content in the composite. For given torch settings, therefore, the simulator may be used to arrive at optimum consolidation strategies to maximize the product quality in terms of increased bond strength and reduced void content.

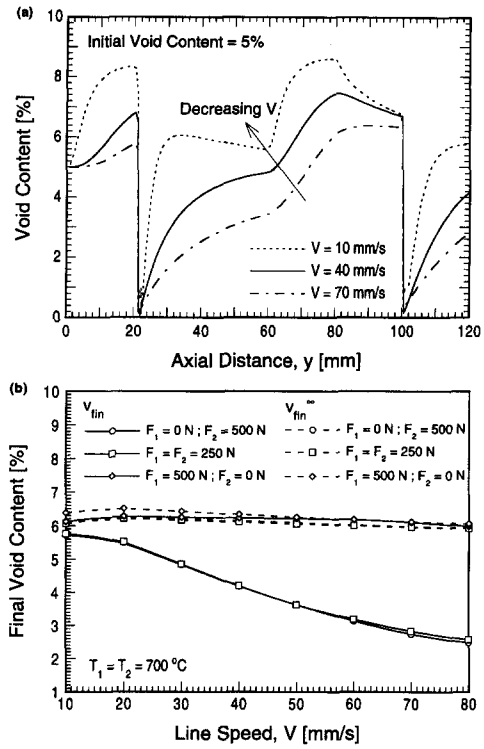

Fig. 5. (a) Variation of the steady state void content in the topmost layer of the composite directly underneath the placement head for three different processing speeds; (b) effect of consolidation forces on the final void content (v_{fin}) and the equilibrium void fraction (v_{fin}^{∞}).

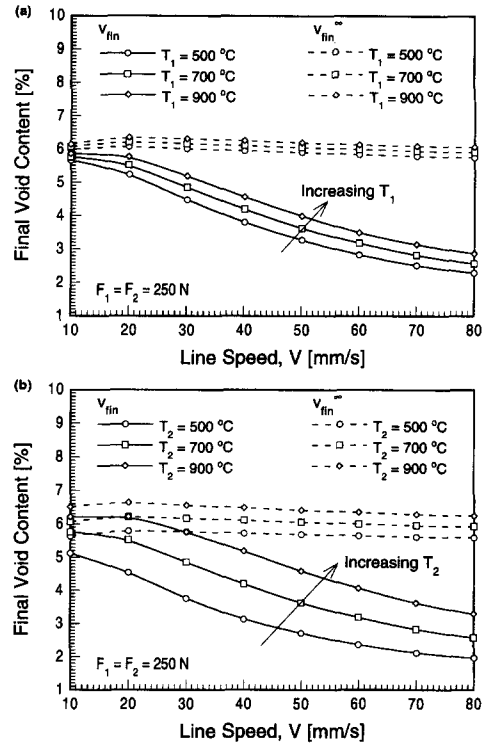

Fig. 6. Effect of (a) preheater and (b) main heater torch temperature on the final void content (v_{fin}) and the equilibrium void fraction (v_{fin}^{∞}).

5.2. *Void dynamics*

The foregoing discussion concerned the composite bond strength, which is one of the parameters characterizing the composite quality. The effects of the processing conditions on the second quality parameter of interest in this study, namely the void content, are examined in the remainder of this section, in Figs. 5–7.

Figure 5(a) shows the variation of the void volume fraction in the tow region directly underneath the placement head, for three different line speeds, consolidation under both the rollers, and moderate torch settings. Starting with an initial void content of 5%, the void fraction is seen to increase under the preheater and main heater torches, and drop sharply under the consolidation rollers ($y \approx 20$ mm and $y \approx 100$ mm, respectively). Beyond the second consolidation roller ($y > 100$), the residual thermal energy in the tows causes the void fraction to increase again. The void fractions are especially higher at the lower line speeds owing to the longer residence time under the torches, as well as the longer times available for void growth beyond the second roller exit. At higher speeds, the shorter residence times under the torches lead to reduced tow temperatures, which coupled with the shorter time available for void growth in the region following Roller 2 results in a decreased final void content. Further, note that the

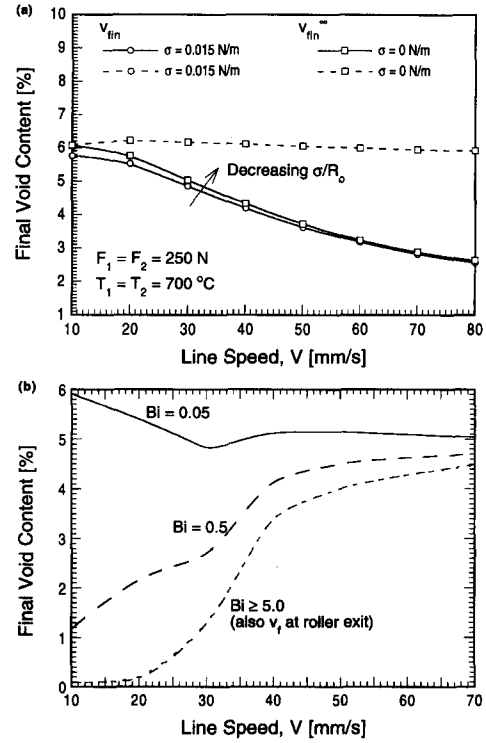

Fig. 7. Effect of (a) surface tension on the final void content (v_{fin}) and the equilibrium void fraction (v_{fin}^{∞}) and (b) convective cooling of the tows downstream of the second consolidation roller (Roller 2 in Fig. 1), on the final void content in the composite.

void fractions at the exit of the consolidation zones are on the order of 0.1%, while the final void content in the tows are much higher owing to the void growth in the regions outside the rollers. This suggests that estimation of the void content based on a void consolidation analysis alone may, in general, be inaccurate.

Since the final void content [which in this study is taken to be the void fraction at the exit of the placement head region, i.e. at $y = 120$ mm in Fig. 1(a)] is of importance from a product quality standpoint, the remainder of the discussion will be in terms of the final quantity. Figure 5(b) demonstrates the effects of three distributions of a total consolidation force of 500 N between the two consolidation rollers. Also plotted in the figure are the equilibrium void fractions, $v_{\mathrm{fin}}^{\infty}$, defined as the void fractions that result if the void internal pressure (p_g) were let to equilibrate with the ambient pressure (p_{atm}) throughout the process. Mathematically, this corresponds to solving the void dynamics equation [equation (9)] with $p_g = p_{\mathrm{atm}}$, for the void radius, and using equation (12) to determine the void fraction. The equilibrium void fraction denotes an upper bound on the void content in the tows and may be used as a quick guideline in process design.

Figure 5(b) shows that the two cases, (i) consolidation with equal forces on the two rollers and (ii) consolidation under the second roller alone, yield the same final void content in the product. The decrease in the final void content with increasing line speed is a result of the reduced tow temperatures and the smaller times available for void growth. Also, the equilibrium void fraction is seen to remain more or less constant at about 6% over the entire range of line speeds studied. The case of consolidation under the first roller alone, amounts to prolonged exposure of the tows to high temperatures without subsequent consolidation, resulting in higher void content in the final product. In fact, the void fraction is seen to approach the upper bound, which it may be noted is higher than the initial void content, for all line speeds.

As may be apparent in the foregoing discussion, the heating of the tows plays an important role in both the void consolidation and void growth processes. The individual effects of the preheater and main torches are examined in Fig. 6. Figure 6(a) reveals that as the preheater torch temperature is increased, the void fraction in the final product increases, as expected. The equilibrium void fraction, $v_{\mathrm{fin}}^{\infty}$, which is a function of the tow temperatures, also increases slightly with the increase in T_t. Figure 6(b) exhibits trends that are generally similar to those in Fig. 6(a). However, noteworthy in Fig. 6(b) is the more pronounced influence of the main heater torch temperature in comparison with the preheater torch temperature [cf. Fig. 6(a)]. This may be explained by considering the effects of the main torch, which is a primary factor determining the residual temperatures in the region beyond the exit of the second roller [$y > 100$ mm in Fig. 2(a)]. A higher value of the main torch temperature therefore results in a much higher void fraction as compared to a similar value of the preheater torch temperature.

The results on the void content presented thus far have been based on a constant value of surface tension ($=0.015$ N m^{-1}) between the void and the polymer melt. This value of $\sigma = 0.015$ N m^{-1} corresponds to a tow melt temperature of 320°C (an estimate of the typical temperatures under the roller for nominal process settings) and was obtained using the temperature-dependent relationship given in ref. [22]. Physically, the surface tension decreases with increasing temperatures. Since this temperature dependence was not accounted for in the present analysis, the influence of surface tension as a parameter on the final void fraction was assessed for an extreme setting of $\sigma = 0$ N m^{-1}. Figure 7(a) presents the resulting effect, from which it may be inferred that surface tension plays a relatively minor role in the consolidation and void growth processes, and that the assumption of a constant, temperature-independent surface tension is a reasonable one.

The convective cooling of the tows in the region beyond the exit of the second consolidation roller is an important parameter affecting the residual temperature and hence the final void content in the tows. The profiles in Figs. 2(a) and 5(a) suggest that a significantly reduced void content could be achieved in the product if the tows were cooled through forced convection, downstream of the second consolidation roller. In fact, in the limit of an instantaneous cooling of the tow ($h = \infty$), the void content in the product may be 'frozen' at the value at the exit of the consolidation roller, where the lowest void fraction is realized during the process. With this motivation, a parametric study was conducted in terms of a top surface cooling Biot number (defined as $Bi = h_t \cdot H/k_z$) in the range $0.05 \leqslant Bi < \infty$.

The results of the study are summarized in Fig. 7(b) which shows the final void content as a function of the line speed and the Biot number. It is seen that for small values of the Biot number (as in the case of the natural convective cooling considered in results presented previously), the void content *decreases* with increasing line speed owing to the reduced time available for void growth downstream of the roller at higher speeds. However, as the Biot number is increased, the tow temperatures drop quickly resulting in a smaller increase in the void content beyond the roller exit. This causes a reversal in the trend in the void fraction variation with respect to the line speed at moderate to high Biot numbers. For these Biot numbers, the void fraction increases with increasing line speeds owing to the reduced time available for consolidation under the roller. At very high Biot numbers ($Bi \approx \infty$), the tow is instantaneously cooled to the ambient temperature (which is less than the glass transition temperature), and the void fraction at the exit of the roller is preserved through the remainder

of the process. The results in Fig. 7(b) suggest that active cooling of the tows beyond the consolidation roller may be necessary for producing quality parts.

The results presented in this section clearly demonstrate that void growth contributes significantly to the final void content, and that an estimation of the void content accounting for the void consolidation process alone could lead to considerably lower estimates of the composite void fraction. It is evident from the void fraction results that lower temperatures of the main heater torch coupled with a rapid cooling of the tows beyond the exit of the second roller may be used to obtain reduced void content in the composite. However, it was also seen that higher torch temperatures are required to achieve good bond strength in the composite. Similarly, although use of Roller 1 alone for compaction yields improved interfacial bonding [Fig. 4(b)], it is the least attractive configuration from the viewpoint of the final void content, as seen in Fig. 5(b). Selection of the optimal processing conditions therefore requires a careful consideration of these trade-offs simultaneously.

The analysis presented in this paper focused on the interlaminar bond strength and the void content in the composite as the two main product quality parameters. For a realistic process design, however, other factors such as polymer degradation, dimensional changes, and residual stresses must also be considered concurrently in arriving at overall optimum process configurations. Identification of processing windows and optimal process settings, based on practical considerations and using the theoretical models presented herein is addressed in a separate work [23], which the interested reader is referred to for details.

6. CONCLUSIONS

The mechanisms of bond strength development, and void consolidation and growth during thermoplastic tow-placement with on-line consolidation were studied. Theoretical models were developed for the heat transfer, void consolidation and growth phenomena involved in the process. A process simulator employing these models along with models for the mechanisms of intimate contact and polymer healing was described. A bond strength model coupling the interactions between the phenomena of intimate contact and healing was described, and an approximate expression for the dimensionless bond strength was derived based on simplifying assumptions. Parametric studies were carried out using the integrated process simulator to investigate the effects of the line speed, compaction force, torch temperatures, and placement head configuration on the consolidation process, primarily in terms of the degree of bonding and the final void content in the product.

It was generally seen that bonding in the composite was maximized over an optimum range of line speed, which shifted towards lower values as the numbers of layers in the composite increased. Increasing the compaction force was shown to improve the product quality by increasing the degree of bonding and reducing the final void content in the composite. Increasing the heat input from the torches improved the degree of bonding, but resulted in a higher final void content if the tows were let to cool by natural convection beyond the exit of the consolidation roller. Of the two heat sources, however, the main heater torch was seen to have a more pronounced effect on both the degree of bonding and the void content. A modification of the head configuration to provide compaction under two rollers was found to improve the effectiveness of the process considerably. It was further noted that forced cooling of the tows beyond the consolidation zone may be necessary to obtain parts with low void content. Overall, the study presented important insights towards better designing and engineering the two-placement process with on-line consolidation.

Acknowledgements—This work was supported in part by the U.S. Army Research Office through award DAAH04-94-G-0285 (the RAPTECH-ACM program). Content of the information does not necessarily reflect the position or the policy of the Government, and no official endorsement shall be inferred.

REFERENCES

1. M. A. Lamontia, M. B. Gruber, M. A. Smoot, J. Sloan and J. W. Gillespie, Jr, Design, manufacture and testing of AS-4 graphite/PEEK thermoplastic composite 24-inch ring-stiffened cylinder model, *Proceedings of the Submarine Technology Symposium*, The Johns Hopkins University Applied Physics Laboratory (1992).
2. M. A. Lamontia, M. B. Gruber, M. A. Smoot, J. Sloan and J. W. Gillespie, Jr, Performance of a filament wound graphite thermoplastic composite ring-stiffened pressure hull model, *J. Thermoplastic Compos. Mater.* **8**(1), 15–36 (1995).
3. M. N. Nejhad, R. D. Cope and S. I. Güceri, Thermal analysis of *in-situ* thermoplastic composite tape laying, *J. Thermoplastic Compos. Mater.* **4**, 20–45 (1991).
4. E. P. Beyeler and S. I. Güceri, Thermal analysis of laser assisted thermoplastic matrix composite tape consolidation, *J. Heat Transfer* **110**, 424–430 (1988).
5. S. M. Grove, Thermal modeling of tape laying with continuous carbon fiber reinforced thermoplastic, *Composites* **19**(5), 367–375 (1988).
6. B. J. Andersen and J. S. Colton, A study of the lay-up and consolidation of high performance thermoplastic composites. In *Tomorrow's Materials: Today*, Vol. 34, pp. 1952–1963. International SAMPE Series (1990).
7. S. C. Mantell and G. S. Springer, Manufacturing process models for thermoplastic composites, *J. Compos. Mater.* **26**(16), 2348–2377 (1992).
8. V. Agarwal, The role of molecular mobility in the consolidation and bonding of thermoplastic composite materials, Center for Composite Materials Technical Report 91-39, University of Delaware (1991).
9. L. J. Bastien and J. W. Gillespie, Jr, A nonisothermal healing model for strength and toughness of fusion bonded joints of amorphous thermoplastics, *Polymer Engng Sci.* **31**(24), 1720–1730 (1991).
10. W. Schnabel, *Polymer Degradation: Principles and Practical Applications*. Macmillan, New York (1981).
11. M. Day, J. D. Cooney and D. M. Wiles, A kinetic study of the thermal decomposition of poly(aryl–ether–ether–ketone) in nitrogen, *Polymer Engng Sci.* **29**(1), 19–22 (1989).

12. J. D. Nam and J. C. Seferis, Generalized composite degradation kinetics for polymeric systems under isothermal and nonisothermal conditions, *J. Polymer Sci., Part B: Polymer Phys.* **30,** 455–463 (1992).
13. R. C. Don, R. Pitchumani and J. W. Gillespie, Jr, Simulation of the transients in thermoplastic fiber placement. In *Moving Forward with 50 Years of Leadership in Advanced Materials*. International SAMPE Series **39**(1), 1521–1535 (1994).
14. S. Ranganathan, S. G. Advani and M. A. Lamontia, A non-isothermal process model for consolidation and void reduction during *in-situ* tow-placement of thermoplastic composites, *J. Compos. Mater.* **29**(8), 1040–1062 (1995).
15. K. V. Steiner, E. Faude, R. C. Don and J. W. Gilespie, Jr, *Cut and Refeed Mechanics for Thermoplastic Tape Placement*, Vol. 39, pp. 2627–2636. International SAMPE Series (1994).
16. M. R. Spiegel, *Mathematical Handbook of Formulas and Tables*, Schaum's Outline Series in Mathematics. McGraw-Hill, New York (1968).
17. A. Arefmanesh, S. G. Advani and E. E. Michealides, Numerical study of bubble growth during low pressure structural foam mold filling process, *Proceedings of ANTEC* 89, 47*th Annual Technical Conference of SPE*, p. 883 (1989).
18. C. A. Butler, R. Pitchumani, J. W. Gillespie, Jr and A. G. Wedgewood, Coupled effects of healing and intimate contact on the strength of fusion-bonded thermoplastics, *Proceedings of the 10th Annual ASM/ESD Advanced Composites Conference*, Dearborn, MI, 7–10 November, pp. 595–604 (1994).
19. K. V. Steiner, B. M. Bauer, R. Pitchumani and J. W. Gillespie, Jr, An experimental verification of modeling and control for thermoplastic tape placement, *Proceedings of the SAMPE International Conference*, Anaheim, CA, April, pp. 1550–1559 (1995).
20. S. V. Patankar, *Numerical Heat Transfer and Fluid Flow*. Hemisphere, Washington D.C. (1980).
21. I. Y. Chang and B. S. Haiao, Thermal properties of high performance thermoplastic composites based on poly(ether ketone ketone), 36*th International SAMPE Symposium Proceedings* (1991).
22. J. Brandrup and E. H. Immergut, *Polymer Handbook* (3rd Edn). Wiley, New York (1989).
23. R. Pitchumani, J. W. Gillespie, Jr and M. A. Lamontia, Design and optimization of a thermoplastic tow-placement process with on-line consolidation, *J. Compos. Mater.* (submitted).